GEOPHYSICS, VOL. 74, NO. 3 (MAY-JUNE 2009); P. E111–E123, 8 FIGS., 1 TABLE.
10.1190/1.3085644

Influence of a pipe tool on borehole modes

Bikash K. Sinha[1], Ergün Şimşek[2], and Sergey Asvadurov[3]

ABSTRACT

A sonic measurements-while-drilling tool consists of acoustic transmitters and receivers mounted on a drill collar that has the form of a thick steel pipe. This mandrel is designed to meet the strength requirements of tough logging conditions encountered in deviated and horizontal drilling. A primary goal of sonic measurement is to estimate formation compressional and shear slownesses that are not affected by the presence of a drill collar. Understanding the basic physics of monopole, flexural, and quadrupole modes in a cylindrically layered structure consisting of a concentric steel pipe in a water-filled borehole can help in estimating formation compressional and shear slownesses from at least one branch, either of the monopole, dipole, or quadrupole family of modes. Results show that coupling between the pipe and formation modes is strongly dependent on formation properties relative to the borehole-fluid compressional slowness. The presence of a steel pipe tool in a borehole causes a significant increase in the Stoneley dispersion at low frequencies. However, the Stoneley slownesses at high frequencies remain essentially the same as those in the open hole without a mandrel. The leaky compressional dispersion in slow formations produced by a monopole source also is perturbed at frequencies where the open-hole leaky compressional and Stoneley-wave dispersions are close to each other. Although there is a strong interference between the pipe and formation flexural modes in fast formations, such interference in slow formations occurs at very low frequencies, and the formation flexural dispersion is less affected by the presence of a drill collar at higher frequencies. Interestingly, the presence of a drill collar in a borehole causes rather small changes in the lowest-order quadrupole dispersion from the case of an open hole without a mandrel. Consequently, quadrupole logging is a preferred choice for estimating the formation shear slowness.

INTRODUCTION

Elastic wave propagation in cylindrical structures has been studied for several decades for a wide range of applications. Starting from fundamental studies of elastic wave propagation in plates and cylinders (Gazis, 1959; Meeker and Meitzler, 1964), there is a significant amount of work on wave propagation in composite cylindrical structures that have applications in the analysis of optical fiber acoustic waveguides (Lai et al., 1971; Jen et al., 1986). Elastic waves propagating through the earth are used routinely to estimate physical properties of the formation (Biot, 1952; Schmitt, 1988, 1993).

A typical sonic measurement consists of a fluid-filled borehole where a source and an array of receivers are placed in the fluid. Three types of sources generally are used: a monopole, a dipole, and a quadrupole. A monopole source excites axisymmetric waves propagating along the borehole, whereas a dipole source directed perpendicular to the borehole axis excites flexural waves propagating along the borehole. Quadrupole transmitters are used in a measurement-while-drilling (MWD) environment because formation quadrupole or screw waves essentially are decoupled from the drill-collar quadrupole modes. All of these axisymmetric ($n = 0$), flexural ($n = 1$), and screw ($n = 2$) waves in a borehole are dispersive.

Cheng and Toksöz (1981) used the variational principle to understand the effects of radial layering on guided waves. Tubman et al. (1984), Baker (1984), and Burns et al. (1985) studied full-waveform acoustic logging in radially layered boreholes (with steel casing or cement). Lee (1991) developed a low-frequency approximation for a drill pipe in a fluid-filled borehole. Sinha et al. (1992) and Plona et al. (1992) presented a theoretical and experimental study of axisymmetric wave propagation in fluid-filled cylindrical shells. Subse-

Manuscript received by the Editor 12 June 2008; revised manuscript received 27 October 2008; published online 27 March 2009.
[1]Schlumberger-Doll Research, Cambridge, Massachusetts, U.S.A. E-mail: sinha1@slb.com.
[2]Formerly Schlumberger-Doll Research, Cambridge, Massachusetts, U.S.A.; presently Bahcesehir University, Istanbul, Turkey. E-mail: ergun.simsek@bahcesehir.edu.tr.
[3]Formerly Schlumberger-Doll Research, Cambridge, Massachusetts, U.S.A.; presently McKinsey & Company, Moscow, Russia. E-mail: Sergey_Asvadurov@mckinsey.com.

quently, Hsu et al. (1997) and Rama Rao and Vandiver (1999) reported on axisymmetric modes of an elastic or poroelastic mandrel in a liquid-filled borehole surrounded by a formation.

The presence of a poroelastic mandrel causes a significant attenuation of Stoneley modes that is useful in the design of sonic imaging tools. The lowest-order axisymmetric Stoneley mode dispersion might be utilized to estimate formation shear slowness under favorable conditions (Stevens and Day, 1986). However, a preferable way of determining the formation shear slowness is to measure borehole flexural dispersion using a dipole source and an array of receivers in a liquid-filled borehole in the absence of any significant coupling between pipe and formation flexural modes. The flexural dispersion asymptotically approaches the formation shear-wave speed at low frequencies.

Recently, Sinha and Asvadurov (2004) obtained velocity dispersions and radial depths of investigation at various frequencies for higher-order modes of a water-filled borehole (without a pipe mandrel) in fast and slow formations. Higher-order quadrupole modes could have advantages in the estimation of formation shear slownesses in the presence of a pipe mandrel. The peak excitation of this mode occurs at somewhat higher frequencies than that of the flexural mode and is less susceptible to interference from the pipe quadrupole mode and possible drilling noise.

This paper describes a fundamental study of modal propagation of higher-order modes in cylindrical structures and investigates the effect of interaction of steel pipe dispersion with that of the formation. It is helpful to study such interactions by analyzing first the modal dispersions of components of the coupled system separately. To this end, we analyze the modal dispersion of a fluid-filled borehole in a formation and, separately, a steel pipe immersed in an infinite fluid. Modal dispersions of these two canonical cases provide insight into modal dispersions of the coupled system consisting of a pipe in a fluid-filled borehole, as shown in Figure 1. Hence, a major objective of this paper is to emphasize that coupling between the pipe and formation flexural modes is strongly dependent on formation properties relative to the borehole-fluid compressional slowness.

Numerical solutions are obtained for these structures in terms of dispersion curves for families of monopole (n = 0), flexural (n = 1), and quadrupole (n = 2) modes in the frequency range of interest. Attenuation of the leaky modes also is computed directly from the imaginary part of the complex frequency for cases when they exist.

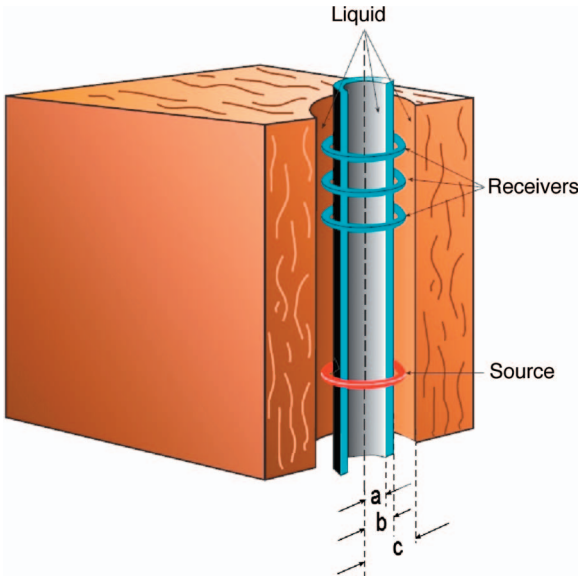

Figure 1. A concentric pipe in a fluid-filled borehole.

MATHEMATICAL FORMULATION

This section contains a brief review of the equations of motion for a cylindrical structure, which are the building blocks of more complex cylindrically layered systems. When referred to the coordinate system shown in Figure 1, the equations of motion for harmonic waves in cylindrical structures can be given by (Gazis, 1959)

$$\rho\ddot{u}_r = \frac{\partial \tau_{rr}}{\partial r} + \frac{1}{r}\frac{\partial \tau_{r\theta}}{\partial \theta} + \frac{\partial \tau_{rz}}{\partial z} + \frac{\tau_{rr} - \tau_{\theta\theta}}{r},$$

$$\rho\ddot{u}_\theta = \frac{1}{r}\frac{\partial \tau_{\theta\theta}}{\partial \theta} + \frac{\partial \tau_{z\theta}}{\partial z} + \frac{\partial \tau_{r\theta}}{\partial r} + 2\frac{\tau_{r\theta}}{r},$$

$$\rho\ddot{u}_z = \frac{\partial \tau_{rz}}{\partial r} + \frac{1}{r}\frac{\partial \tau_{z\theta}}{\partial \theta} + \frac{\partial \tau_{zz}}{\partial z} + \frac{\tau_{rz}}{r}, \qquad (1)$$

where τ_{rr}, $\tau_{\theta\theta}$, τ_{zz}, τ_{rz}, $\tau_{r\theta}$, and $\tau_{z\theta}$ are the stress components; u_r, u_θ, and u_z are the displacement components; and ρ is the mass density of the material of the cylindrical structure at hand.

The constitutive relations for a homogeneous, elastic, and isotropic material are

$$\tau_{rr} = \lambda\Delta + 2\mu\varepsilon_{rr}, \quad \tau_{\theta\theta} = \lambda\Delta + 2\mu\varepsilon_{\theta\theta},$$
$$\tau_{zz} = \lambda\Delta + 2\mu\varepsilon_{zz}, \quad \tau_{r\theta} = 2\mu\varepsilon_{r\theta},$$
$$\tau_{z\theta} = 2\mu\varepsilon_{z\theta}, \quad \tau_{rz} = 2\mu\varepsilon_{rz}, \qquad (2)$$

where $\Delta = \partial u_r/\partial r + u_r/r + (1/r)\partial u_\theta/\partial\theta + \partial u_z/\partial z$; ε_{rr}, $\varepsilon_{\theta\theta}$, $\varepsilon_{r\theta}$, $\varepsilon_{z\theta}$, and ε_{rz} are the strain components; and λ and μ are the Lamé constants for the material of the cylindrical structure at hand.

The strain-displacement relations in cylindrical coordinates take the form

$$\varepsilon_{rr} = \frac{\partial u_r}{\partial r}, \quad \varepsilon_{\theta\theta} = \frac{1}{r}\frac{\partial u_\theta}{\partial\theta} + \frac{u_r}{r},$$
$$\varepsilon_{zz} = \frac{\partial u_z}{\partial z}, \quad \varepsilon_{r\theta} = \frac{1}{2}\left[\frac{1}{r}\frac{\partial u_r}{\partial\theta} + \frac{\partial u_\theta}{\partial r} - \frac{u_\theta}{r}\right],$$
$$\varepsilon_{z\theta} = \frac{1}{2}\left[\frac{1}{r}\frac{\partial u_z}{\partial\theta} + \frac{\partial u_\theta}{\partial z}\right], \quad \varepsilon_{rz} = \frac{1}{2}\left[\frac{\partial u_z}{\partial r} + \frac{\partial u_r}{\partial z}\right]. \qquad (3)$$

An eigensolution to any linear elastodynamic solution can be expressed in terms of a scalar potential ϕ and a vector potential $\mathbf{H}$,

$$\mathbf{u} = \nabla\phi + \nabla\times\mathbf{H}, \qquad (4)$$

where $\nabla\cdot\mathbf{H}$ is arbitrary, and

$$V_1^2\nabla^2\phi = -\omega^2\phi,$$
$$V_2^2\nabla^2\mathbf{H} = -\omega^2\mathbf{H}. \qquad (5)$$

We can express the displacement components in cylindrical coordinates in terms of these scalar and vector potentials:

$$u_r = \frac{\partial \phi}{\partial r} + \frac{1}{r}\frac{\partial H_z}{\partial \theta} - \frac{\partial H_\theta}{\partial z},$$
$$u_\theta = \frac{1}{r}\frac{\partial \phi}{\partial \theta} + \frac{\partial H_r}{\partial z} - \frac{\partial H_z}{\partial z},$$
$$u_z = \frac{\partial \phi}{\partial z} + \frac{\partial H_\theta}{\partial r} + \frac{H_\theta}{r} - \frac{1}{r}\frac{\partial H_r}{\partial \theta}. \quad (6)$$

Substituting these displacement components into the constitutive relations and the stress equations of motion, we can write equation 5 in the following form in terms of the scalar potential ϕ and three components of vector potential $\mathbf{H}$:

$$-\frac{\omega^2}{V_1^2}\phi = \frac{\partial^2 \phi}{\partial r^2} + \frac{1}{r}\frac{\partial \phi}{\partial r} + \frac{1}{r^2}\frac{\partial^2 \phi}{\partial \theta^2} + \frac{\partial^2 \phi}{\partial z^2},$$
$$-\frac{\omega^2}{V_2^2}H_r = \frac{\partial^2 H_r}{\partial r^2} + \frac{1}{r}\frac{\partial H_r}{\partial r} + \frac{1}{r^2}\left(\frac{\partial^2 H_r}{\partial \theta^2} - 2\frac{\partial H_\theta}{\partial \theta} - H_r\right) + \frac{\partial^2 H_r}{\partial z^2},$$
$$-\frac{\omega^2}{V_2^2}H_\theta = \frac{\partial^2 H_\theta}{\partial r^2} + \frac{1}{r}\frac{\partial H_\theta}{\partial r} + \frac{1}{r^2}\left(\frac{\partial^2 H_\theta}{\partial \theta^2} + 2\frac{\partial H_r}{\partial \theta} - H_\theta\right) + \frac{\partial^2 H_\theta}{\partial z^2},$$
$$-\frac{\omega^2}{V_2^2}H_z = \frac{\partial^2 H_z}{\partial r^2} + \frac{1}{r}\frac{\partial H_z}{\partial r} + \frac{1}{r^2}\frac{\partial^2 H_z}{\partial \theta^2} + \frac{\partial^2 H_z}{\partial z^2}. \quad (7)$$

A solution of equation 7 can be written in the form

$$\phi = f(r)\cos n\theta e^{i\zeta z},$$
$$H_r = h_r(r)\sin n\theta e^{i\zeta z},$$
$$H_\theta = h_\theta(r)\cos n\theta e^{i\zeta z},$$
$$H_z = h_z(r)\sin n\theta e^{i\zeta z}, \quad (8)$$

which satisfies equation 7 provided that

$$\frac{\partial^2 f}{\partial r^2} + \frac{1}{r}\frac{\partial f}{\partial r} + \left(\frac{\alpha^2 - n^2}{r^2}\right)f = 0, \quad (9)$$

$$\frac{\partial^2 h_z}{\partial r^2} + \frac{1}{r}\frac{\partial h_z}{\partial r} + \left(\frac{\beta^2 - n^2}{r^2}\right)h_z = 0, \quad (10)$$

$$\frac{\partial^2 h_r}{\partial r^2} + \frac{1}{r}\frac{\partial h_r}{\partial r} + \frac{1}{r^2}(-n^2 h_r + 2nh_\theta - h_r) + \beta^2 h_r = 0, \quad (11)$$

$$\frac{\partial^2 h_\theta}{\partial r^2} + \frac{1}{r}\frac{\partial h_\theta}{\partial r} + \frac{1}{r^2}(-n^2 h_\theta + 2nh_r - h_\theta) + \beta^2 h_\theta = 0, \quad (12)$$

where

$$\alpha^2 = \frac{\omega^2}{V_1^2} - \zeta^2, \quad \beta^2 = \frac{\omega^2}{V_2^2} - \zeta^2, \quad (13)$$

where V_1 and V_2 are the compressional- and shear-wave velocities, respectively.

Subtracting and adding equations 11 and 12, we obtain

$$\frac{\partial^2 h_1}{\partial r^2} + \frac{1}{r}\frac{\partial h_1}{\partial r} + \left(\beta^2 - \frac{(n+1)^2}{r^2}\right)h_1 = 0,$$
$$\frac{\partial^2 h_2}{\partial r^2} + \frac{1}{r}\frac{\partial h_2}{\partial r} + \left(\beta^2 - \frac{(n-1)^2}{r^2}\right)h_2 = 0, \quad (14)$$

where

$$2h_1 = h_r - h_\theta, \quad 2h_2 = h_r + h_\theta. \quad (15)$$

Solutions of equations 9, 10, 14, and 15, respectively, can be written in the form

$$f = AJ_n(\alpha r) + BY_n(\alpha r), \quad (16)$$

and

$$h_z = h_3 = A_3 J_n(\beta r) + B_3 Y_n(\beta r), \quad (17)$$

$$2h_1 = h_r - h_\theta = 2A_1 J_{n+1}(\beta r) + 2B_1 Y_{n+1}(\beta r), \quad (18)$$

$$2h_2 = h_r + h_\theta = 2A_2 J_{n-1}(\beta r) + 2B_2 Y_{n-1}(\beta r), \quad (19)$$

where J_n and Y_n are nth-order Bessel functions of the first and second kind.

Because $\nabla \cdot \mathbf{H}$ is arbitrary, we can eliminate one h_i. Following the work of Gazis (1959), we set $h_2 = 0$, and from equations 18 and 19, we have

$$h_r = h_1, \quad h_\theta = -h_1. \quad (20)$$

The solution for the displacement components now can be written

$$u_r = \left(\frac{\partial f}{\partial r} + \frac{n}{r}h_3 + i\zeta h_1\right)\cos n\theta e^{i\zeta z},$$
$$u_\theta = \left(\frac{-n}{r}f + i\zeta h_1 - \frac{\partial h_3}{\partial r}\right)\sin n\theta e^{i\zeta z},$$
$$u_z = \left(i\zeta f - \frac{\partial h_1}{\partial r} - (n+1)\frac{h_1}{r}\right)\cos n\theta e^{i\zeta z}. \quad (21)$$

Substitution of equations 16–20 into 21 yields the following expressions for the displacement components in the mth cylindrical layer that can be used to satisfy the appropriate boundary conditions:

$$u_r = \left[\left\{\frac{n}{r}J_n(\alpha_{(m)}r) - \alpha_{(m)}J_{n+1}(\alpha_{(m)}r)\right\}A^{(m)} + \left\{\frac{n}{r}Y_n(\alpha_{(m)}r) - \alpha_{(m)}Y_{n+1}(\alpha_{(m)}r)\right\}B^{(m)} + i\zeta J_{n+1}(\beta_{(m)}r)A_1^{(m)} + i\zeta Y_{n+1}(\beta_{(m)}r)B_1^{(m)}\right.$$

$$+\frac{n}{r}J_n(\beta_{(m)}r)A_3^{(m)} + \frac{n}{r}Y_n(\beta_{(m)}r)B_3^{(m)}\Bigg]\cos n\theta e^{i(\omega t+\zeta z)}, \quad (22)$$

$$u_\theta = \Bigg[\Bigg[-\frac{n}{r}J_n(\alpha_{(m)}r)\Bigg]A^{(m)} + \Bigg[-\frac{n}{r}Y_n(\alpha_{(m)}r)\Bigg]B^{(m)} + [i\zeta J_{n+1}(\beta_{(m)}r)]A_1^{(m)} + [i\zeta Y_{n+1}(\beta_{(m)}r)]B_1^{(m)} + \Bigg\{-\frac{n}{r}J_n(\beta_{(m)}r) + \beta_{(m)}J_{n+1}(\beta_{(m)}r)\Bigg\}A_3^{(m)} + \Bigg\{-\frac{n}{r}Y_n(\beta_{(m)}r) + \beta_{(m)}Y_{n+1}(\beta_{(m)}r)\Bigg\}B_3^{(m)}\Bigg]\cos n\theta e^{i(\omega t+\zeta z)}, \quad (23)$$

$$u_z = [\{i\zeta J_n(\alpha_{(m)}r)\}A^{(m)} + \{i\zeta Y_n(\alpha_{(m)}r)\}B^{(m)} - [\beta_{(m)}J_n(\beta_{(m)}r)]A_1^{(m)} - \{\beta_{(m)}Y_n(\beta_{(m)}r)\}B_1^{(m)}]\cos n\theta e^{i(\omega t+\zeta z)}, \quad (24)$$

where the index m denotes the mth cylindrical layer parameter and

$$\alpha_{(m)}^2 = \frac{\omega^2}{V_{1(m)}^2} - \zeta^2, \quad \beta_{(m)}^2 = \frac{\omega^2}{V_{2(m)}^2} - \zeta^2, \quad (25)$$

with $V_{1(m)}$ and $V_{2(m)}$ the compressional- and shear-wave velocities for the mth media.

At this point, it should be noted that the solutions given by equations 22–24 are valid for a solid annulus. The corresponding solution for a solid rod is obtained simply by discarding the terms containing $Y_n(\alpha r)$ or $Y_n(\beta r)$, which diverge as $r\to 0$. On the other hand, the wave solution in a solid formation of infinite radial extent takes the form (Auld, 1973; Aki and Richards, 1980)

$$u_r = \Bigg[\Bigg\{\frac{n}{r}H_n(\alpha r) - \alpha H_{n+1}(\alpha r)\Bigg\}A^{(m)} + [i\zeta H_{n+1}(\beta r)]A_1^{(m)} + \Bigg[\frac{n}{r}H_n(\beta r)\Bigg]A_3^{(m)}\Bigg]\cos n\theta e^{i(\omega t+\zeta z)}, \quad (26)$$

$$u_\theta = \Bigg[\Bigg\{-\frac{n}{r}H_n(\alpha r)\Bigg\}A^{(m)} + [i\zeta H_{n+1}(\beta r)]A_1^{(m)} + \Bigg[-\frac{n}{r}H_n(\beta r) + \beta H_{n+1}(\beta r)\Bigg]A_3^{(m)}\Bigg]\sin n\theta e^{i(\omega t+\zeta z)}, \quad (27)$$

$$u_z = [\{i\zeta H_n(\alpha r)\}A^{(m)} - \{\beta H_n(\beta r)\}A_1^{(m)}]\cos n\theta e^{i(\omega t+\zeta z)}, \quad (28)$$

where $H_n(x)$ represents the outgoing Hankel functions of the second kind consistent with the $\exp(i\omega t)$ given by

$$H_n(x) = J_n(x) - iY_n(x). \quad (29)$$

The corresponding displacement components in an inviscid fluid take the reduced form

$$u_r^f = \Bigg\{\Bigg[\frac{n}{r}J_n(\alpha^f r) - \alpha^f J_{n+1}(\alpha^f r)\Bigg]C_1^{(m)} + \Bigg[\frac{n}{r}Y_n(\alpha^f r) - \alpha^f Y_{n+1}(\alpha^f r)\Bigg]C_2^{(m)}\Bigg\} \times \cos n\theta e^{i(\omega t+\zeta z)}, \quad (30)$$

$$u_\theta^f = \Bigg\{-\frac{n}{r}[J_n(\alpha^f r)C_1^{(m)} + Y_n(\alpha^f r)C_2^{(m)}]\Bigg\}\sin n\theta e^{i(\omega t+\zeta z)}, \quad (31)$$

$$u_z^f = i\zeta[J_n(\alpha^f r)C_1^{(m)} + Y_n(\alpha^f r)C_2^{(m)}]\cos n\theta e^{i(\omega t+\zeta z)}, \quad (32)$$

where

$$\alpha^f = \frac{\omega^2}{V_f^2} - \zeta^2, \quad (33)$$

V_f represents the compressional-wave velocity in the fluid, and the superscript f refers to that quantity or parameter associated with the fluid medium.

At this point, it should be noted that the solution given by equations 30–32 is valid for a liquid annulus. The corresponding solution for a liquid column is obtained simply by discarding the terms containing $Y_{0,1}(\alpha^f r)$, which diverge as $r\to 0$. On the other hand, the wave solution in a fluid medium of infinite radial extent takes the form

$$u_r^f = -\alpha^f H_{n+1}(\alpha^f r)D_1^{(m)}\cos n\theta e^{i(\omega t+\zeta z)}, \quad (34)$$

$$u_\theta^f = \Bigg\{-\alpha^f H_{n+1}(\alpha^f r) + \frac{n}{r}H_n(\alpha^f r)\Bigg\}D_1^{(m)}\sin n\theta e^{i(\omega t+\zeta z)}, \quad (35)$$

$$u_z^f = i\zeta H_n(\alpha^f r)D_1^{(m)}\cos n\theta e^{i(\omega t+\zeta z)}. \quad (36)$$

The classical boundary conditions at a fluid-solid interface are given by

$$\begin{bmatrix}\tau_{rr}^{(1)}\\ \tau_{r\theta}^{(1)}\\ \tau_{rz}^{(1)}\\ u_r^{(1)}\end{bmatrix}_{r=a} = \begin{bmatrix}\tau_{rr}^{(2)}\\ \tau_{r\theta}^{(2)}\\ \tau_{rz}^{(2)}\\ u_r^{(2)}\end{bmatrix}_{r=a}, \quad (37)$$

where the superscripts 1 and 2 refer to the media on either side of the surface of discontinuity $r = a$. However, it should be noted that the shear stresses $\tau_{rz}^{(1)}$ and $\tau_{r\theta}^{(1)}$ in an inviscid fluid are identically equal to

zero. At a solid-solid interface, the continuity conditions are

$$\begin{bmatrix} \tau_{rr}^{(1)} \\ \tau_{r\theta}^{(1)} \\ \tau_{rz}^{(1)} \\ u_r^{(1)} \\ u_\theta^{(1)} \\ u_z^{(1)} \end{bmatrix}_{r=a} = \begin{bmatrix} \tau_{rr}^{(2)} \\ \tau_{r\theta}^{(2)} \\ \tau_{rz}^{(2)} \\ u_r^{(2)} \\ u_\theta^{(2)} \\ u_z^{(1)} \end{bmatrix}_{r=a}, \quad (38)$$

whereas the normal stress components are set equal to zero at traction-free surfaces.

The unknown amplitudes associated with different cylindrical layers are determined by satisfying the boundary conditions at the relevant interfaces. The solution to a cylindrically layered system can be obtained by satisfying appropriate boundary conditions at all liquid-solid or solid-solid interfaces. These conditions can be expressed in terms of a matrix equation $\mathbf{Lc} = \mathbf{0}$, where the vector $\mathbf{c}$ denotes the unknown amplitude coefficients as follows:

$$\mathbf{c} = (A^{(1)}, A^{(2)}, B^{(2)}, A_1^{(2)}, B_1^{(2)}, \times A_3^{(2)}, B_3^{(2)}, A^{(3)}, B^{(3)}, A^{(4)}, A_1^{(4)}, A_3^{(4)})^T. \quad (39)$$

For nontrivial solutions of this matrix equation, we require that the determinant of coefficient matrix $\mathbf{L}$ be zero.

A search routine can be established to find the resonant mode velocities (V) for a given frequency (f) in an (f,V) search domain. Here, we have a slightly different search domain consisting of nondimensional frequency Ω and nondimensional axial wavenumber ζ, where $\Omega = \omega c/V_{2(4)}$ and $\zeta = kc$, which are converted to (f,V) by using

$$V = \Omega V_{2(4)}/\zeta, \quad f = \Omega V_{2(4)}/2\pi c, \quad (40)$$

where $\omega = 2\pi f$ is the radial frequency, $c = r_3$ is the borehole radius, k is the resonant mode axial wavenumber, and $V_{2(4)}$ is the formation shear velocity in the 4^{th} cylindrical layer. Figure 2 contains an illustration of the conversion from one domain to another for a flexural mode.

COMPUTATIONAL RESULTS

Sinha and Asvadurov (2004) present a detailed analysis of monopole, dipole, and quadrupole modes of a water-filled borehole in an infinite formation. In this work, we describe computational results for the two additional configurations to study effects of the mandrel or an equivalent pipe on the borehole modes. The two configurations are (1) a steel pipe in an infinite liquid, and (2) a steel pipe in a water-filled borehole surrounded by a fast/slow formation. A fast or slow formation refers to the formation shear-wave speed being faster or slower than the compressional-wave speed in the borehole fluid, which is water in all cases. Parameters for the materials appearing in our investigation are given in Table 1. The assumed geometric parameters for an MWD tool are as follows: the borehole radius is $c = 13$ cm (5 inches); the pipe inner and outer radii are $a = 6.5$ cm and $b = 10$ cm (or 2.5 inches and 4 inches, respectively).

To check the accuracy of our formulation and implementation, we first obtain borehole slowness dispersions by using the dyadic Green's function formulation of Lu and Liu (1994). This formulation yields synthetic waveforms at an array of receivers produced by a monopole, dipole, or quadrupole source placed on the borehole axis. Synthetic waveforms then are processed by a modified matrix pencil algorithm (Hua and Sarkar, 1990) to isolate nondispersive and dispersive arrivals in the wavetrain. For this problem, we use 20 receivers placed in the annulus between the drill collar and a fast formation (see Table 1 for material properties). The distance between the source and first (last) receiver is 0.6 m (3 m). Figure 3 shows the recorded synthetic waveforms and slowness dispersions obtained by processing these waveforms obtained from a monopole source (top row) and a dipole source (bottom row). In dispersion plots, we also depict the mode-search algorithm (black solid lines) results that confirm a very good agreement between these two formulations.

Computational results consist of (1) modal dispersion, (2) radiation-induced attenuation, and (3) radial variation of modal amplitudes at select frequencies. The dashed horizontal lines in dispersion plots correspond to the compressional, shear, and liquid slownesses, labeled C, S, and L, respectively. In the case of a pipe in infinite liquid, these correspond to the compressional and shear slownesses of steel; in the case of a pipe in a water-filled borehole in an infinite formation, they correspond to the slownesses of the formation. The vertical solid lines in modal amplitude plots denote radial locations of the inner and outer surfaces of the pipe, and the borehole surface, respectively.

We choose the frequency range of 1 through 15 kHz that covers the common frequency range of interest for various measurements made while drilling, and we present results for the Stoneley, flexural, and quadrupole modes in this frequency range. For some of these modes, we compute the amplitude of the radial component of particle acceleration on the axis $r = 0$, and the excitation function, as defined in Sinha et al. (1994); black solid and red dashed lines depict U_r and U_z acceleration components, respectively. To obtain a complete

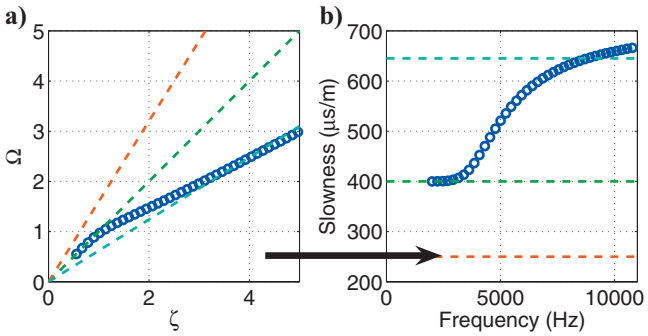

Figure 2. (a) Blue circles denote zeros of boundary condition determinant matrix in (Ω,ζ) space. Red, green, and cyan dashed lines show formation compressional, shear, and fluid compressional velocities, respectively. (b) Slowness-frequency dispersion $(1/V,f)$ obtained from results in Figure 2a.

Table 1. Material parameters for cylindrical components

Material	V_1 (m/s)	V_2 (m/s)	ρ (kg/m^3)
Fast formation	3658	2032	2350
Slow formation	1890	508	2054
Steel	5800	3100	7900
Water	1500	—	1000

understanding of such modes, we also present the corresponding displacement and stress profiles at chosen frequencies.

Figures 4–6 contain computational results for these configurations: (1) a steel pipe in infinite liquid, (2) a concentric steel pipe in a water-filled borehole surrounded by a fast formation, and (3) a concentric steel pipe in a water-filled borehole surrounded by a slow formation.

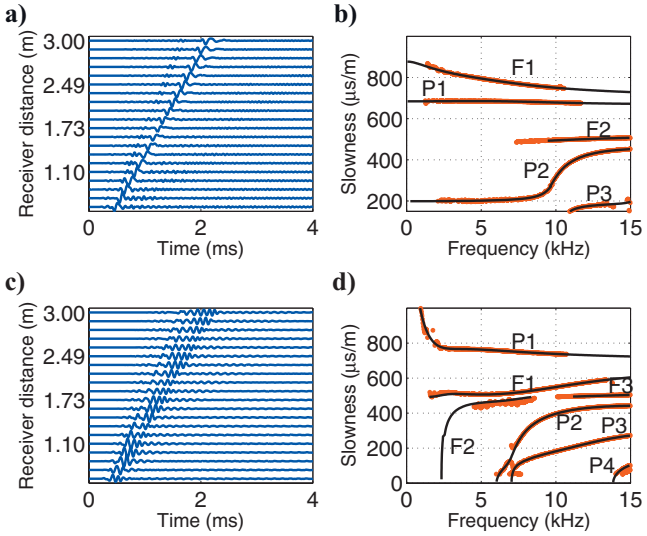

Figure 3. (a) Synthetic waveforms generated by a dyadic Green's function method of Lu and Liu (1994) for a monopole source; (b) modal dispersions obtained by processing synthetic waveforms by a modified matrix pencil algorithm (red dots) and a mode-search algorithm (solid black lines); (c) and (d) follow the same notation as (a) and (b), respectively, for a dipole source.

Steel pipe in infinite liquid

A major objective of studying dispersions of a solid pipe in infinite liquid is to help recognize them in the composite system of a pipe inside a fluid-filled borehole surrounded by a formation. To this end, we need to look at such details as the profiles of the slowness dispersion curves, the cutoff frequencies of the various modes, and the magnitudes of the attenuations. Plona et al. (1992) and Aristégui et al. (2001) studied and reported on this particular case. In this section, we describe results for a steel pipe in infinite liquid, as shown in Figures 4a-c, 5a-c, and 6a-c.

Monopole slowness dispersions

Figure 4a shows the four monopole modes in the frequency range of interest. One mode is barely visible at the high-frequency end. The first mode, labeled m = 1, is nonradiating, has slowness (phase and group) close to the fluid speed, and is almost nondispersive, as shown in Figure 4b. The second mode, m = 2, is the pipe extensional mode, which is essentially nondispersive at lower frequencies as high as 7 kHz. The third and fourth modes have cutoff frequencies of approximately 10 and 15 kHz and are moderately attenuative. Figure 4c presents the excitation spectra of the first two modes, m = 1,2. The excitation spectra are plotted in terms of radial and axial (U_r and U_z are shown by solid black and dashed red curves, respectively) acceleration components on the borehole axis, as discussed by Sinha and Asvadurov (2004).

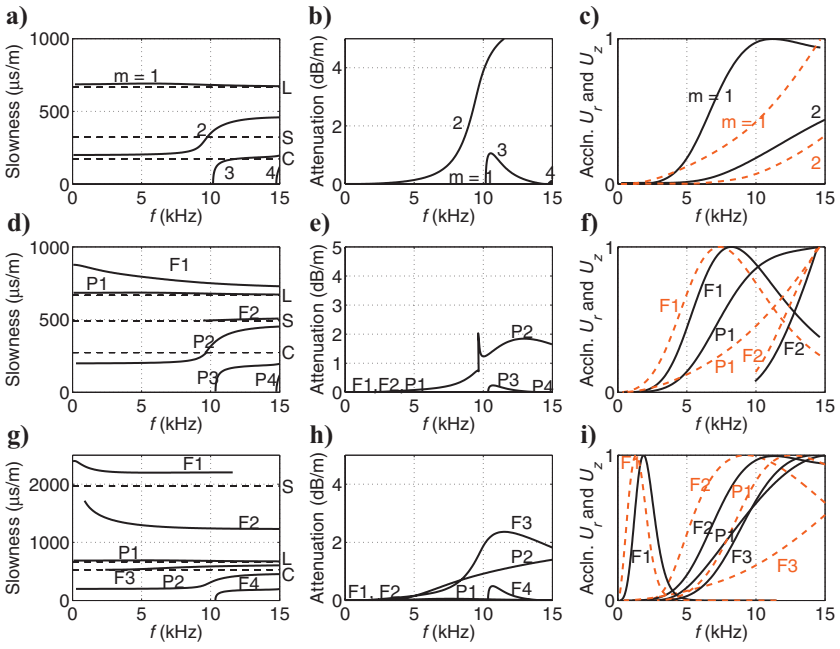

Figure 4. Monopole modes: Phase slowness dispersion curves (left column), radiation-induced attenuation (center column), and excitation spectra (right column) of a steel pipe in liquid (top row), a concentric steel pipe in a water-filled borehole surrounded by a fast formation (center row), and a concentric steel pipe in a water-filled borehole surrounded by a slow formation (bottom row). In the right column, U_r and U_z are shown by solid black and dashed red curves, respectively.

Dipole slowness dispersions

The flexural dispersions for a steel pipe in infinite liquid are presented in Figure 5a. Figure 5b shows that all the modes exhibit varying degrees of attenuation, except in the low-frequency range below 2 kHz where the first mode, m = 1, has slownesses larger than the slowness of the fluid. As frequency goes to zero, the slowness of this first mode increases without bound. The higher-order m = 2, 3, and 4 are cutoff modes with relatively high group velocity and with cutoff frequencies of approximately 6, 7, and 14 kHz. Figure 5c shows the excitation spectra for the steel pipe lowest-order flexural formation mode (n = 1;m = 1), and a higher-order pipe flexural mode (n = 1;m = 2).

Quadrupole slowness dispersions

The quadrupole modes for a pipe in infinite fluid are presented in Figure 6a. All of these are cutoff modes with cutoff frequencies of approximately 3, 3.5, 11.5, and 12 kHz. The high-frequency asymptote of the first mode is the slowness of the liquid, and the dispersion curve for this mode shows a characteristic cusp at approximately 7 kHz. It appears that the lowest-order quadrupole mode of the steel pipe (in vacuum) and that

of the liquid column are crossing each other, causing a strong interaction around 7 kHz. When the phase slowness is smaller than the fluid compressional slowness, all such modes radiate energy into the surrounding liquid. Figure 6b illustrates radiation-induced attenuation of these modes as a function of frequency. Figure 6c shows the excitation function for the lowest-order nonradiating formation quadrupole modes (n = 2; m = 1 and 2). Unlike the lowest-order monopole and flexural modes, even the lowest-order quadrupole mode exhibits a cutoff frequency at about 3 kHz.

Steel pipe in a borehole surrounded by a fast formation

The behavior of modes of a composite structure of steel pipe in a fluid-filled borehole might or might not be similar to the behavior of corresponding modes in disjoint structures of the pipe in infinite liquid and the fluid-filled borehole without a tool. In this section, we describe results for a steel pipe in a fluid-filled borehole surrounded by a fast formation as shown in Figures 4d-f (monopole), 5d-f (dipole), and 6d-f (quadrupole). We follow a notation that a mode preceded by F or P denotes a mode dominated by formation or pipe properties, respectively.

Monopole slowness dispersions

The monopole modes in this configuration are presented in Figure 4d. Comparing results in Figure 4d for the case of a pipe in a borehole and a pipe immersed in an infinite liquid, we observe that the lowest-order modes are only slightly perturbed, and we recognize the slower of the two as the formation Stoneley, and the faster of the two as the first monopole pipe mode. Accordingly, in Figure 4d we label these two modes as F1 for the first formation mode and P1 as the first pipe mode. The pipe mode is pushed closer to the liquid head wave, and the Stoneley F1 mode is repelled by the faster mode to the higher slowness range (in particular, the low-frequency slowness of the Stoneley mode increases to above 800 μs/m), but otherwise the shape of the two modes remains unchanged.

In the next mode, we recognize the perturbed shape of the second, pseudo-Rayleigh, formation mode and label it F2. The cutoff frequency of this mode increases from about 6 kHz to about 9.5 kHz. The mode gets repelled to the faster side toward the shear slowness of the formation. These effects need to be taken into account for accurate interpretation; in particular, this will influence the process of proper frequency range selection for formation shear inversion.

Figure 4e shows that F1, P1, and F2 modes do not radiate energy into the surrounding formation. In the next mode, which we label P2, we clearly see the second pipe mode that is undisturbed by the presence of the formation. This mode is lightly attenuative.

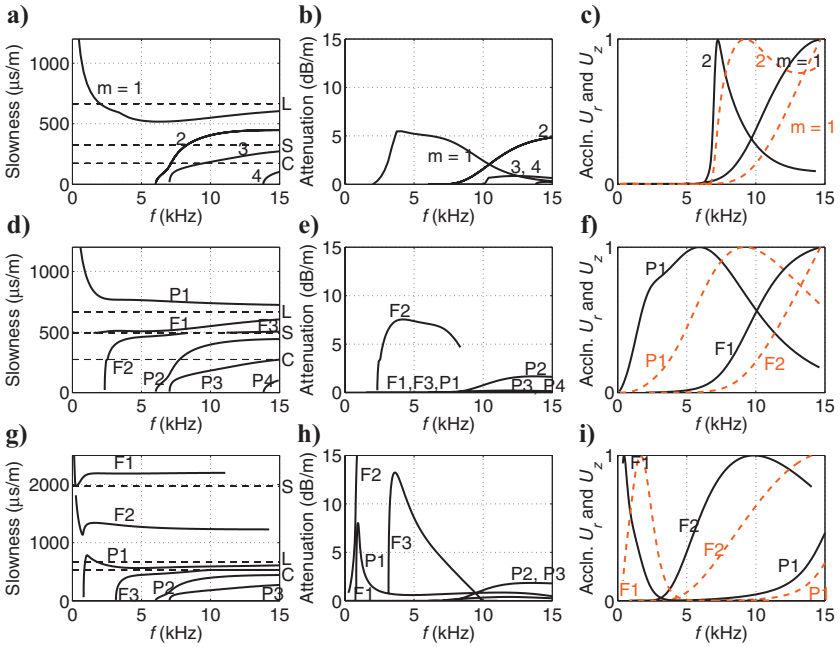

Figure 5. Flexural Modes: Phase slowness dispersion curves (left column), radiation-induced attenuation (center column), and excitation spectra (right column) of a steel pipe in liquid (top row), a concentric steel pipe in a water-filled borehole surrounded by a fast formation (center row), and a concentric steel pipe in a water-filled borehole surrounded by a slow formation (bottom row). In the right column, U_r and U_z are shown by solid black and dashed red curves, respectively.

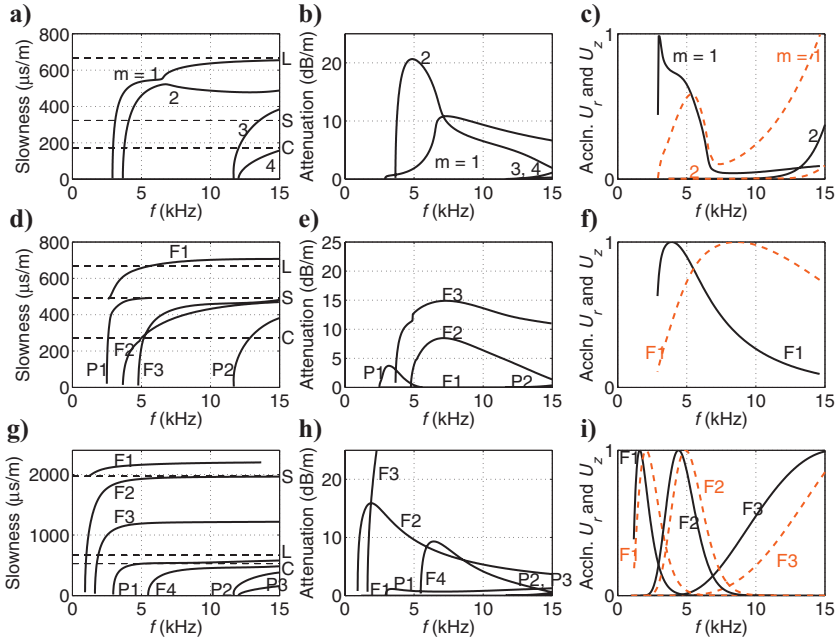

Figure 6. Quadrupole modes: Phase slowness dispersion curves (left column), radiation-induced attenuation (center column), and excitation spectra (right column) of a steel pipe in liquid (top row), a concentric steel pipe in a water-filled borehole surrounded by a fast formation (center row), and a concentric steel pipe in a water-filled borehole surrounded by a slow formation (bottom row). In the right column, U_r and U_z are shown by solid black and dashed red curves, respectively.

The higher-order modes P3 and P4 are almost undisturbed modes m = 3 and 4 of the pipe. The higher-order formation modes are not present in this frequency range.

The signal received at an array of receivers can be represented by a convolution of source spectrum and modal excitation functions (Sinha et al., 1994). In Figure 4f, we show the modal excitation spectra for the three lowest modes, for which excitation of the mode labeled F1 resembles the pipe lowest-order mode with the excitation peak moved to a slightly lower frequency.

Dipole slowness dispersions

Seven modes enter the picture for the dipole dispersion curves in our composite structure; see Figure 5d. The slowest two provide examples of the interesting interaction of the lowest-order pipe and formation modes. At the low-frequency range, the mode labeled P1 behaves as the lowest-order pipe mode, m = 1, hence the label we assign to it. However, as frequency increases as high as above 5 kHz, the behavior of P1 starts to differ from that of the pipe mode, and the high-frequency behavior of this composite mode is similar to that of the lowest-order formation mode, m = 1. On the other hand, the second composite mode F1 starts out as the lowest-order formation mode, m = 1, but as frequency increases, its behavior reflects that of the lowest-order pipe mode. This type of interaction of modes of the separate structures is common when the separate modes cross each other if the two figures are overlaid. Obviously, in the composite structure the modes cannot cross each other in the complex plane because this would lead to nonuniqueness of the solution, so they either repel each other or interact in ways just described.

Modes labeled F3 and F4 are the perturbed m = 3 and 4 modes of the borehole without a tool. The mode F4 has a higher cutoff frequency than in the case without a tool. This behavior is similar to the monopole case described above. The mode F3 gets displaced by the proximity of the modified F1 mode. The rest of the modes are almost nonperturbed pipe modes P2, P3, and P4.

Figure 5e shows that F1, P1, and F4 modes do not radiate energy into the surrounding formation. Figure 5f shows the modal excitation spectra for the two lowest flexural modes.

Quadrupole slowness dispersions

The quadrupole family of modes shown in Figure 6d exhibits negligible interference with steel pipe quadrupole modes. In the slowest mode, F1, we recognize the first quadrupole mode of the borehole without a tool. This mode is perturbed and has the cutoff frequency of approximately 3 kHz, instead of the 5 kHz as in the case of an empty borehole in an infinite formation.

Four cutoff modes appear in the picture. The modes F2 and F3 follow the behavior of the second and third modes of the borehole without a tool. In particular, they cross in the phase slowness plane, similarly to the case without a tool (note that there is no crossing in the complex plane and hence no contradiction to the uniqueness.) However, the high-frequency behavior of the F3 mode differs from that of the independent system in that it now does not cross the shear slowness within the frequency range of our interest. The mode with the cutoff frequency of 2.5 kHz is labeled P1 because it behaves similarly to the low-frequency part of the first quadrupole mode of the pipe in infinite liquid. However, unlike the independent mode in Figure 6e, this composite mode disappears when it crosses the shear slowness of the formation. The last mode in the current picture has the behavior similar to the second pipe mode and is labeled P2. The third pipe mode, as well as the fourth and fifth formation modes, does not appear in the figure.

Figure 6f shows that all the modes except F1 are dispersive.

Steel pipe in a borehole surrounded by a slow formation

Modal dispersions associated with a slow formation in the presence of a steel pipe are significantly different from those in a fast formation. In this section, we study these differences and provide useful guidelines for proper processing and interpretation of sonic data.

Monopole slowness dispersions

The monopole modes in this configuration are presented in Figure 4g. Comparing results in Figure 4g for the case of a pipe in a borehole and a pipe immersed in an infinite liquid, we notice that the lowest-order Stoneley mode, labeled F1 in the figure, is perturbed greatly by the presence of the pipe. It no longer intersects the formation shear, and its zero frequency limit is altered significantly. The higher formation modes, labeled F2 and F3 in the figure, are not perturbed significantly by the presence of the pipe. The only change is that the leaky compressional mode does not grow in slowness as fast as in the open-hole case, and at the highest frequency that we consider, 15 kHz, is only halfway between the formation compressional slowness and slowness of the fluid, whereas in the open-hole case, at the same frequency the mode was already close to its high-frequency asymptote of the fluid slowness.

The highest formation cutoff mode, which we label F4, is altered by the presence of the pipe in the following way. The cutoff frequency becomes significantly higher, changing from 7 kHz in the open-hole case to more than 10 kHz in the case of the pipe presence, and its slowness value at frequency 15 kHz is almost three times as low as in the open-hole case. The next cutoff formation mode, visible in the open-hole case in our frequency range of interest, does not even show up in the case of the presence of the pipe.

Pipe modes, labeled P1 and P2 in the figure, are not altered significantly compared with the case of the pipe in infinite fluid. These two modes, respectively, correspond to the slow-Stoneley mode (m = 1) and pipe extensional mode (m = 3) in the case of the pipe in infinite liquid. However, the fast-Stoneley mode (m = 2), and pipe cutoff modes m = 3 and m = 4 from the steel pipe in fluid, are not present.

The signal received at an array of receivers can be represented by a convolution of source spectrum and modal excitation functions (Sinha et al., 1994). In Figure 4i, we show modal excitation spectra for the four lowest modes. Comparing results in this figure with those of the other two cases, we notice that the excitation of the modes is not altered significantly.

Dipole slowness dispersions

An extremely interesting slowness dispersion picture for the dipole dispersion curves of our composite structure is presented in Figure 5g. As we can see from overlaying results for the two cases of an open hole without a mandrel and a steel pipe in liquid, the lowest-order pipe dipole mode in its original form intersects two of the formation modes, in their original form. This intersection results in significant alteration of these three modes. This type of interaction of modes of the separate structures is common when the separate modes cross each other if the two figures are overlaid. Obviously, in

the composite structure the modes cannot cross each other in the complex plane because this would lead to nonuniqueness of the solution to $\det(\mathbf{L}) = 0$, so they either repel each other or interact in ways just described. We label the resulting three modes by their high-frequency asymptotes as F1, F2, and P1. In each of these modes, we can observe a characteristic kink that has the approximate frequency of the point where the undisturbed pipe mode would intersect the undisturbed formation modes.

The rest of the formation and pipe modes present in the figure, which are labeled F3, P2, and P3, are relatively unperturbed. Mode m = 4 from the case of the open hole without a mandrel is not present in this frequency range, and is pushed out to higher frequencies by the presence of the higher pipe modes. Figure 5h shows that all the modes except F1 are dispersive. Figure 5i shows the modal excitation spectra for the three lowest flexural modes.

Quadrupole slowness dispersions

The quadrupole family of modes shown in Figure 6g presents a simpler case than the monopole and dipole cases. The modes of the open-hole and pipe families do not seem to be affected greatly by each other. In the slowest mode F1, we recognize the first quadrupole mode of the borehole without a tool. The second and third slowest modes are labeled F2 and F3 and follow the behavior of the second and third modes of the borehole without a tool. The next cutoff mode resembles the first pipe mode and is labeled P1. It should be noted, however, that this mode seems to be interacting with the mode m = 4 of the open-hole case. In particular, at high frequencies it becomes slower than the liquid. We choose to label the modes according to their low-frequency limit. Going through the modes in the order of increasing cutoff frequency, we recognize the next formation mode F3 and two higher-order pipe quadrupole modes P2 and P3. All of these modes seem to be very weakly altered compared with the previous figures. Figure 6h shows that all the modes except F1 are dispersive.

In Figure 6i, we show the modal excitation spectra for the modes F1, F2, and F3. We see that these excitations do not differ significantly from the open-hole case.

Radial variation of modal amplitudes

Radial variation of modal amplitudes provides estimates of radial depth of investigation as a function of frequency. Radial depth of investigation is an indicator of formation volume probed by a given mode at various frequencies. This helps in a proper interpretation of measured borehole dispersions and their subsequent applications in inferring formation mechanical attributes at different radial positions from the borehole surface. Even though we analyze these variations at multiple frequencies, here we describe radial variation of modal displacement amplitudes U_r and U_z, and radial stress τ_{rr}, for the formation Stoneley and pipe extensional, formation flexural and pipe flexural, and formation quadrupole modes at select frequencies.

Fast formation

In Figure 7a and b, we show the modal amplitude profiles at frequencies of 2 (solid lines) and 7 kHz (dashed lines) for the two lowest-order monopole modes labeled F1 and P1, respectively. As expected, lower frequencies exhibit larger radial depth of investigation than higher-frequency signals. We notice that at both frequencies for these modes, the axial displacement in the pipe is rather small. The radial stress associated with these modes extends deeper into the formation for the F1 mode at these two frequencies. Generally, radial depth of investigation at a given frequency is largest for the formation flexural followed by the Stoneley and quadrupole modes.

Figure 7c and d displays modal amplitudes of two lowest-order dipole modes at frequencies of 2 (solid lines) and 7 (dashed lines) kHz. We notice that at 2 kHz, the radial displacement of the pipe is significantly larger for the P1 mode, whereas the penetration of the radial displacement and stress amplitudes into the formation is larger for the F1 mode. At 7 kHz, this distinction appears to vanish. Figure 7d also shows that the relative radial stress component (denoting the hydrostatic pressure in the borehole fluid) inside the pipe is approximately one-tenth of its value in the annulus between the pipe and formation. These results suggest that a hydrophone placed inside the annulus will be far more sensitive, compared with one placed inside the pipe tool, to detecting the pressure signal associated with the formation flexural mode.

In Figure 7e, we show the radial variations of displacement amplitudes at frequencies of 2 (solid lines) and 7 (dashed lines) kHz for the quadrupole F1 mode.

Slow formation

In Figure 8a and b, we show the modal amplitude profiles at frequencies of 1.5 (solid lines) and 5 kHz (dashed lines) for the two lowest-order monopole modes labeled F1 and P1, respectively. For the monopole F1 mode, the depth of investigation into the formation is about 4 borehole radii, and the dominant part of the energy is concentrated inside the annulus between the pipe and the formation, and in the formation itself at 1.5 and 5 kHz. As the frequency increases, the depth of penetration decreases. For the monopole P1 mode, most energy is concentrated inside the pipe and fluid, although some radial displacement is present inside the formation as well. Figure 8c-e displays modal amplitude profiles for the dipole F1, dipole P1, and quadrupole F1 modes, respectively. Interestingly, the quadrupole F1 mode in a slow formation at frequencies of 1.5 and 5 kHz exhibits similar penetration depths as observed in a fast formation at 2 and 7 kHz.

SUMMARY

We have studied the influence of a pipe tool on monopole, dipole, and quadrupole waves in a water-filled borehole. Unlike previous studies, this work uses a complex mode-search routine (based on Muller's technique [Muller, 1956; Atkinson, 1988]) that has the capability of analyzing real and complex modes associated with a fluid-filled borehole in the presence of a thick pipe (or drill collar). Consequently, we identify radiating and nonradiating borehole modes supported by a system of cylindrical structures that are both dispersive and attenuative. Results for modal dispersions, radiation-induced attenuation, and excitation spectra for a few select modes have been obtained for axisymmetric, flexural, and quadrupole modes as high as 15 kHz in fast and slow formations.

In addition to calculating modal dispersions, attenuations, and excitation functions, we plot an acoustic field associated with any of these modes at select frequencies. These plots are extremely useful for a proper interpretation of borehole sonic data in geophysical applications. For instance, these plots indicate radial depth of investigation as a function of sonic logging frequency that can help in confirming if elastic moduli estimated from an MWD sonic tool represent formation properties in the far-field or might have been compro-

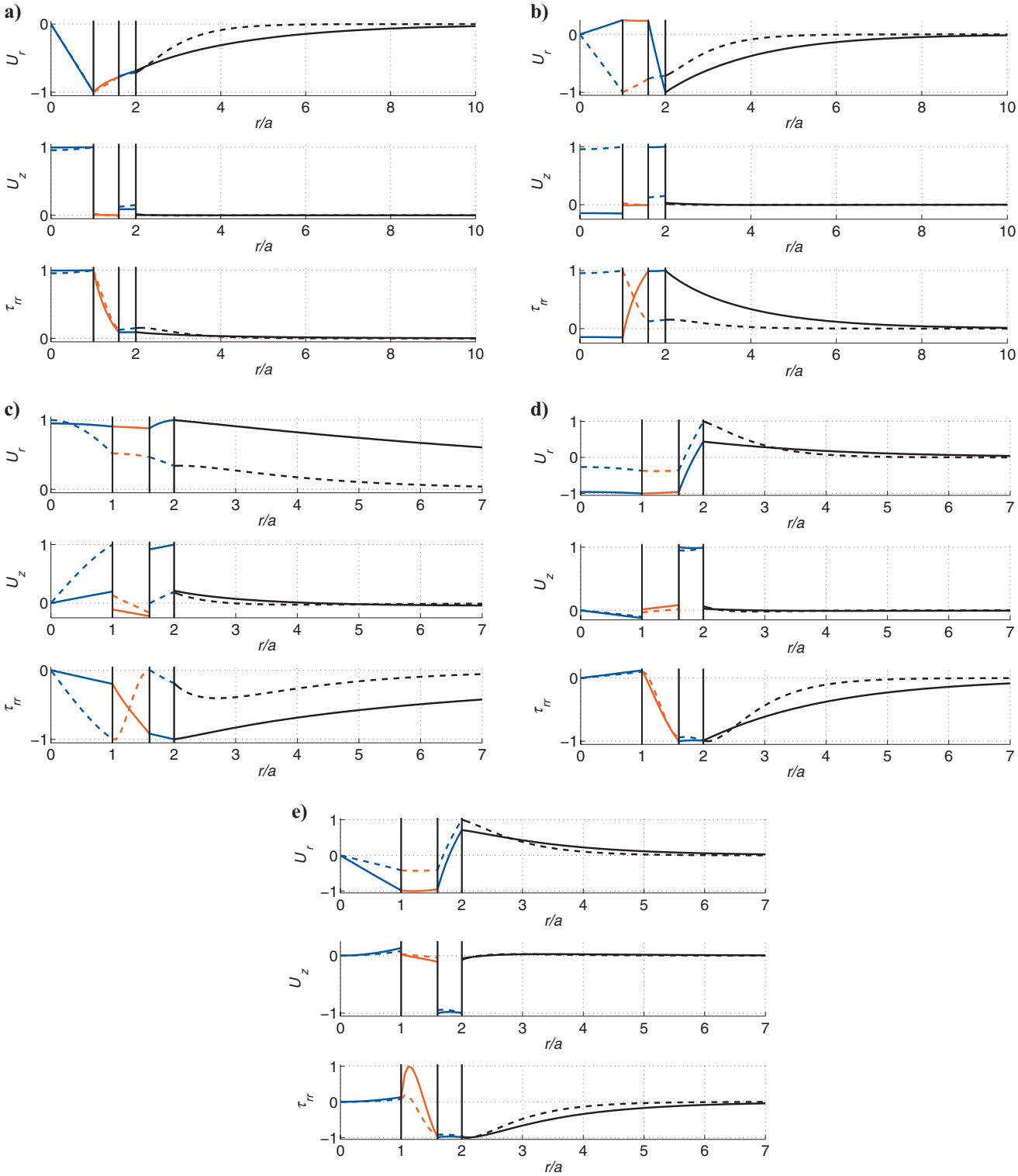

Figure 7. A concentric steel pipe in a water-filled borehole surrounded by a fast formation: Normalized displacements (U_r and U_z) and radial stress (τ_{rr}) plotted as a function of r/a for the mode (a) monopole F1, (b) monopole P1, (c) flexural F1, (d) flexural P1, (e) quadrupole F1. The solid and dashed lines show results for frequencies 2 and 7 kHz, respectively.

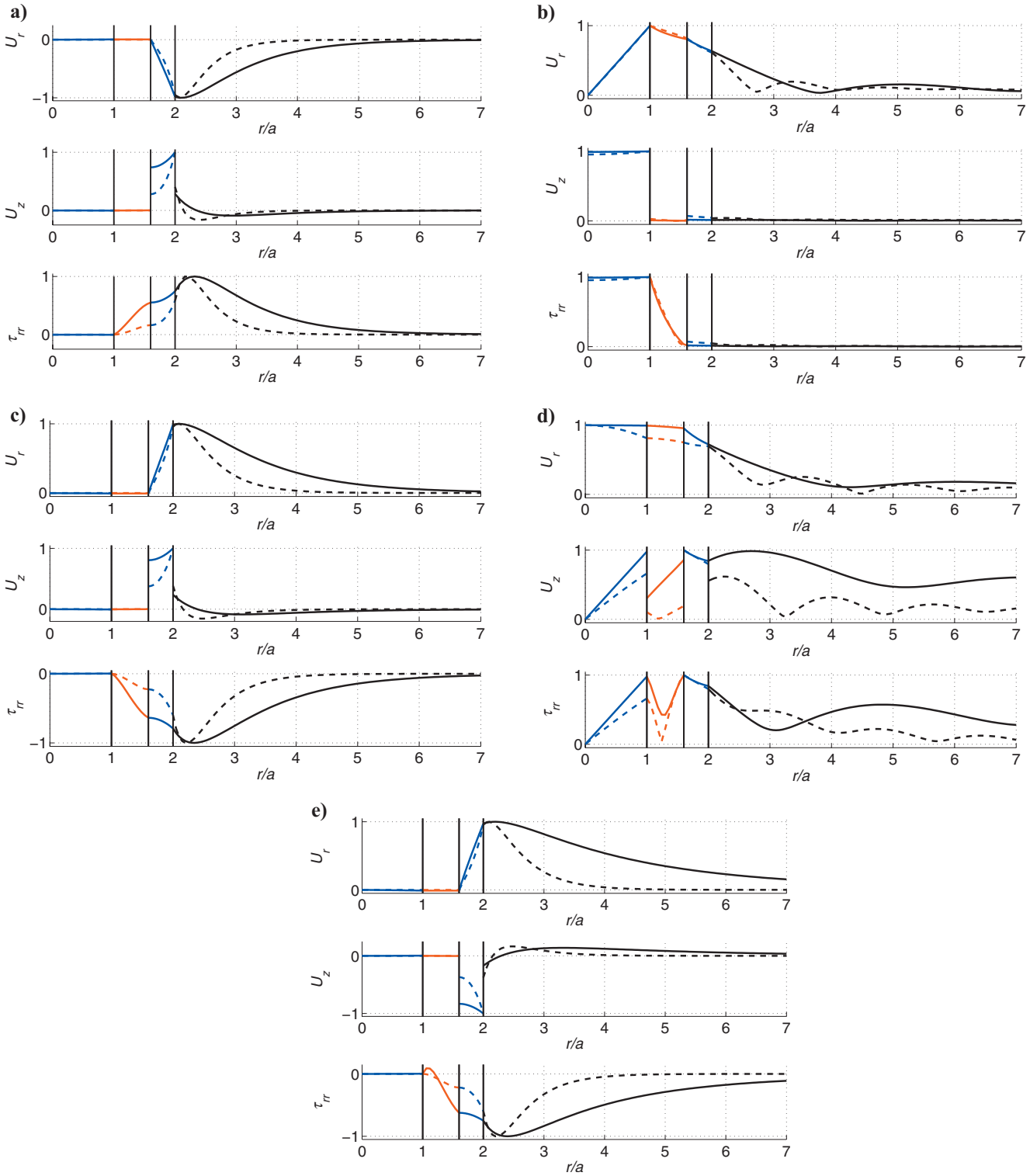

Figure 8. A concentric steel pipe in a water-filled borehole surrounded by a slow formation: Normalized displacements (U_r and U_z) and radial stress (τ_{rr}) plotted as a function of r/a for the mode (a) monopole F1, (b) monopole P1, (c) flexural F1, (d) flexural P1, (e) quadrupole F1. The solid and dashed lines show results for frequencies 1.5 and 5 kHz, respectively.

mised by the near-wellbore alteration caused by stress concentrations or mechanical damage. In addition, this study helps in the design of a sonic tool with proper placement of receivers to maximize sensitivity to a particular borehole mode of interest.

CONCLUSIONS

Important conclusions from this study follow.

1) The radial depths of investigation of the formation Stoneley and flexural modes vary as a function of frequency in a similar fashion. Low frequencies of these modes probe deeper and high frequencies probe shallower into the formation.

   For the fast formation, radial depths of investigation for the Stoneley mode are approximately 5 × borehole radius at 2 kHz, and about 3 × borehole radius at 7 kHz. The radial depth of investigation for the formation flexural mode is approximately 7 × borehole radius at 2 kHz, which is somewhat larger than the Stoneley mode at the same frequency. Similarly, the radial depth of investigation for the pseudo-Rayleigh mode (n = 1; F2) is about 4 × borehole radius at 12 kHz. The radial depth of investigation for the formation quadrupole mode (n = 2) is about 4 × borehole radius at 7 kHz.

   For the slow formation, radial depths of investigation for the Stoneley mode are approximately 6 × borehole radius at 2.5 kHz, and about 3 × borehole radius at 6 kHz. Interestingly, the radial depth of investigation for the monopole leaky compressional mode (n = 0; F3) is about 10 × borehole radius at 6 kHz. The radial depth of investigation for the formation flexural mode is approximately 7 × borehole radius at 2 kHz, which is somewhat larger than the Stoneley mode at the same frequency. The radial variation of modal amplitudes for the lowest-order steel pipe mode (n = 1, F1) at higher frequencies of 2 through 5 kHz exhibits a slow, oscillatory decay into the formation. Note that at these frequencies the pipe mode slownesses are less than the formation shear slowness causing it to radiate energy into the formation. The radial depth of investigation for the formation quadrupole mode (n = 2) is about 5 × borehole radius at 5 kHz.
2) Modal amplitude distributions associated with the formation flexural mode in the presence of a pipe tool suggest that hydrophones placed in the annulus between the pipe and formation generally will be more sensitive to detecting formation arrivals than those placed inside the pipe, where the pressure signal is rather small. This emphasizes the importance of exposing hydrophone detectors to the fluid in the annulus through a slotted pipe.
3) The presence of sleeve/pipe modal dispersions causes significant perturbations in the formation modal dispersions, particularly in the frequency band where the two independent sets of modes are in close proximity or crossing each other.
4) The excitation spectra of the formation modes are mildly affected by the presence of the steel pipe tool, based on a comparison of these results for the case of a fluid-filled borehole in the absence of any tool structure as presented by Sinha and Asvadurov (2004). As mentioned earlier, acoustic signal amplitude at a receiver location is obtained by a convolution of the transmitter (source) pulse and excitation spectrum (which is like an impulse response) of the propagating system. Modal spectra or excitation spectra help in an optimal bandwidth selection of the transmitter for a particular logging.

For example, in the case of Stoneley logging, the modal spectra of the formation and tool suggest that the monopole transmitter bandwidth should be less than 7 kHz for the fast formation and 5 kHz for the slow formation to suppress the excitation of unwanted pipe modes. On the other hand, in the case of compressional head-wave logging (P and S modes), the modal spectra or excitation spectra suggest that two unwanted pipe modes propagating close to the pipe material compressional and shear slownesses are likely to be excited along with formation arrivals in the frequency band above 10 kHz.

There are two choices to deal with such situations. Either we use the processing algorithm to filter out the pipe arrivals, or we limit the monopole transmitter bandwidth to less than 10 kHz even for compressional head-wave logging.

Similarly, modal analyses suggest that the dipole transmitter bandwidth should be below 7 kHz for the fast formation and 5 kHz for the slow formation to suppress the excitation of unwanted flexural pipe modes. Above 10 kHz, both of these pipe flexural modes are likely to be excited, and they must be filtered out by the processing algorithm for proper interpretation of the formation flexural signals.

Interestingly, the pipe quadrupole modes appear to be well separated from the lowest-order formation quadrupole mode (n = 2; F1) in the frequency band below 10 kHz. Therefore, quadrupole logging for estimating the formation shear slowness is preferred in the industry.

REFERENCES

Aki, K., and P. G. Richards, 1980, Quantitative seismology: Theory and methods: W. H. Freeman.

Aristégui, C., M. J. S. Lowe, and P. Cawley, 2001, Guided waves in fluid-filled pipes surrounded by different fluids: Ultrasonics, **39**, 367–375.

Atkinson, K. E., 1988, An introduction to numerical analysis, 2nd ed.: John Wiley and Sons, Inc.

Auld, B. A., 1973, Acoustic fields and waves in solids: John Wiley and Sons, Inc.

Baker, L. J., 1984, The effect of the invaded zone on full wavetrain acoustic logging: Geophysics, **49**, 796–809.

Biot, M., 1952, Propagation of elastic waves in a cylindrical bore containing a fluid: Journal of Applied Physics, **23**, 997–1005.

Burns, D. R., C. H. Cheng, and M. N. Toksöz, 1985, Energy partitioning and attenuation of guided waves in a radially layered borehole: SEG Technical Program Expanded Abstracts, 4, 46–47.

Cheng, C. H., and M. N. Toksöz, 1981, Elastic wave propagation in a fluid-filled borehole and synthetic acoustic logs: Geophysics, **46**, 1042–1053.

Gazis, D., 1959, Three-dimensional investigation of the propagation of waves in hollow circular cylinders: Part 1 — Analytical foundation; Part 2 — Numerical results: Journal of the Acoustical Society of America, **31**, 568–577.

Hsu, C.-J., S. Kostek, and D. Johnson, 1997, Tube waves and mandrel modes: Experiment and theory: Journal of the Acoustical Society of America, **102**, 3277–3289.

Hua, Y., and T. K. Sarkar, 1990, Matrix pencil method for estimating parameters of exponentially damped/undamped sinusoids in noise: IEEE Transactions on Acoustics, Speech, and Signal Processing, **38**, 814–824.

Jen, C., A. Safaai-Jazi, and G. Farnell, 1986, Leaky modes in weakly guiding fiber acoustic waveguides: IEEE Transactions on Ultrasonics, Ferroelectrics, and Frequency Control, **33**, 634–643.

Lai, J., E. Dowell, and T. Tauchert, 1971, Propagation of harmonic waves in a composite elastic cylinder: Journal of the Acoustical Society of America, **49**, 220–227.

Lee, H. Y., 1991, Drillstring axial vibration and wave propagation in boreholes: Ph.D. thesis, Massachusetts Institute of Technology.

Lu, C., and Q. Liu, 1994, Three-dimensional dyadic Green's function for elastic waves in multilayer cylindrical structures: Journal of the Acoustical Society of America, **96**, 3337–3338.

Meeker, T., and A. Meitzler, 1964, Guided wave propagation in elongated cylinders and plates: Academic Press.

Muller, D. E., 1956, A method for solving algebraic equations using an automatic computer: Mathematical Tables and Other Aids to Computation, **10**, 208–215.
Plona, T., B. K. Sinha, S. Kostek, and S. Chang, 1992, Axi-symmetric wave propagation in fluid-loaded cylindrical shells: Part 2 — Theory versus experiment: Journal of the Acoustical Society of America, **92**, 1144–1155.
Rama Rao, V. N., and J. K. Vandiver, 1999, Acoustics of fluid-filled boreholes with pipe: Guided propagation and radiation: Journal of the Acoustical Society of America, **105**, 3057–3066.
Schmitt, D., 1988, Shear wave logging elastic formations: Journal of the Acoustical Society of America, **84**, 2215–2229.
——–, 1993, Dipole logging in cased boreholes: Journal of the Acoustical Society of America, **93**, 640–657.
Sinha, B. K., and S. Asvadurov, 2004, Dispersion and radial depth of investigation of borehole modes: Geophysical Prospecting, **52**, 271–286.
Sinha, B. K., A. Norris, and S. Chang, 1994, Borehole flexural modes in anisotropic formations: Geophysics, **59**, 1037–1052.
Sinha, B. K., T. Plona, S. Kostek, and S. Chang, 1992, Axi-symmetric wave propagation in fluid-loaded cylindrical shells: Part 1 — Theory: Journal of the Acoustical Society of America, **92**, 1132–1143.
Stevens, J., and S. Day, 1986, Shear velocity logging in slow formations using the Stoneley wave: Geophysics, **51**, 137–147.
Tubman, K. M., C. H. Cheng, and M. N. Toksöz, 1984, Synthetic full waveform acoustic logs in cased boreholes: Geophysics, **49**, 1051–1059.